Single-molecule chemical denaturation of riboswitches

Paul A. Dalgarno[1], Jorge Bordello[1], Rhodri Morris[1], Patrick St-Pierre[2], Audrey Dubé[2], Ifor D. W. Samuel[1], Daniel A. Lafontaine[2],* and J. Carlos Penedo[1,3,*]

[1]SUPA, School of Physics and Astronomy, University of St Andrews, St Andrews, Fife, KY16 9SS, UK, [2]RNA Group, Département de biologie, Faculté des sciences, Université de Sherbrooke, Sherbrooke, Québec, J1K 2R1, Canada and [3]Biomedical Sciences Research Complex, University of St Andrews, St Andrews, Fife, KY16 9SS, UK

ABSTRACT

To date, single-molecule RNA science has been developed almost exclusively around the effect of metal ions as folding promoters and stabilizers of the RNA structure. Here, we introduce a novel strategy that combines single-molecule Förster resonance energy transfer (FRET) and chemical denaturation to observe and manipulate RNA dynamics. We demonstrate that the competing interplay between metal ions and denaturant agents provides a platform to extract information that otherwise will remain hidden with current methods. Using the adenine-sensing riboswitch aptamer as a model, we provide strong evidence for a rate-limiting folding step of the aptamer domain being modulated through ligand binding, a feature that is important for regulation of the controlled gene. In the absence of ligand, the rate-determining step is dominated by the formation of long-range key tertiary contacts between peripheral stem-loop elements. In contrast, when the adenine ligand interacts with partially folded messenger RNAs, the aptamer requires specifically bound Mg^{2+} ions, as those observed in the crystal structure, to progress further towards the native form. Moreover, despite that the ligand-free and ligand-bound states are indistinguishable by FRET, their different stability against urea-induced denaturation allowed us to discriminate them, even when they coexist within a single FRET trajectory; a feature not accessible by existing methods.

INTRODUCTION

The application of single molecule techniques to investigate the structure and folding of biomolecules including nucleic acids and proteins has revolutionized our understanding of their biological function (1,2). Interestingly, single-molecule fluorescence-based studies of RNA and protein dynamics have been developed following two different approaches. For proteins, single-molecule studies have predominantly used denaturant agents such as urea and guanidium chloride to reveal the unfolding mechanism and the rate-limiting steps for several proteins (3,4). In contrast, single-molecule studies of RNA dynamics have almost exclusively focused on the effect of metal ions in the RNA secondary and tertiary structure (5,6); although denaturing agents have already been applied to a number of RNA molecules in ensemble-averaging studies (7,8), no equivalent approach has been reported at single-molecule level.

Metabolite-sensing cis-acting RNA elements, so-called riboswitches, are attracting increasing interest, not only because of their growing functional importance in bacterial gene regulation (9–13) but also because they constitute evolutionary optimized model systems to understand the intrinsic plasticity and functional diversity of RNA (9,14). Riboswitches often undergo complex conformational changes induced either by Mg^{2+} ions, ligand-binding or both; therefore, understanding the dynamic nature of

these RNAs has become a key to understand their regulatory function (15). Among these RNA structures, the adenine riboswitch has become a paradigm for the study of RNA-ligand interactions, and it has been the subject of extensive investigations by us and others at ensemble (16–21) and single-molecule molecule level (22–25). In the present work, we have used the sensing domain of the adenine riboswitch as a model system to demonstrate that the combination of single-molecule Förster resonance energy transfer (FRET), and chemical denaturation provides a more powerful platform to investigate RNA dynamics and extract information that otherwise will remain hidden with current single-molecule methods.

Riboswitches are typically positioned within the 5′-untranslated region of messenger RNA (mRNA) and control the expression of genes downstream of the mRNA sequence as well as at more remote locations (9,10,12, 13,26). They are typically composed of two domains: a highly conserved metabolite-sensor, the aptamer domain, and the expression platform (10,12,15) (Figure 1a).
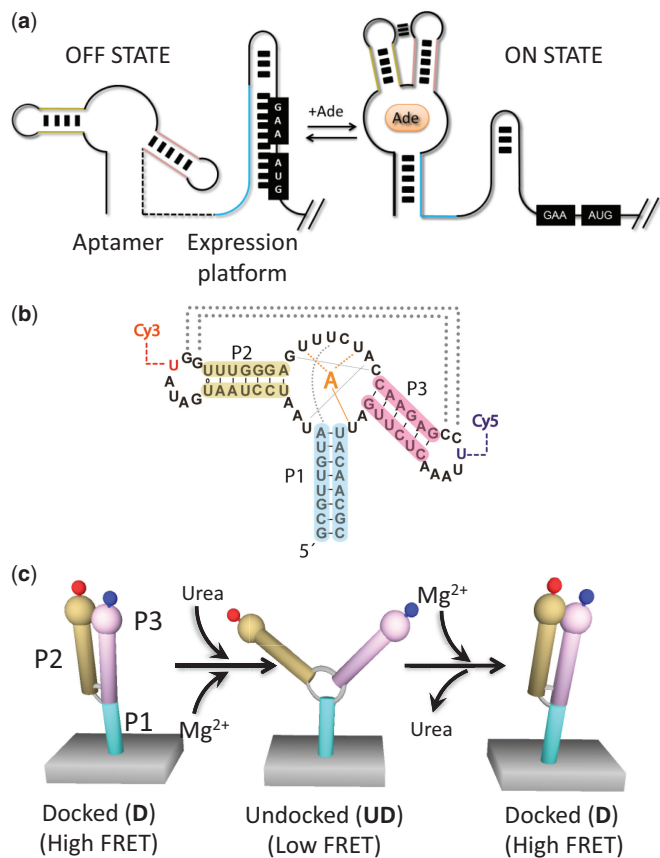

Figure 1. (**a**) Schematic showing control of gene expression by the *V. vulnificus add* riboswitch at the translational level on adenine (Ade) binding. (**b**) Schematic showing the network of interactions within the aptamer core involved in ligand recognition (orange) and in the stabilization of the native state (grey). Base-pair contacts responsible for the P2–P3 loop–loop interaction are shown along with the position of the nucleotides carrying the donor (Cy3) and acceptor (Cy5) FRET pair. (**c**) Adenine aptamers labelled with Cy3 (red) and Cy5 (blue) dyes at specific positions of the P2 and P3 stem loops report conformational changes associated with the docking/undocking process induced by Mg^{2+} ions and urea, respectively.

The secondary structure of the expression platform, which can adopt two mutually exclusive conformations depending on metabolite binding to the aptamer domain, determines the outcome of the regulation process (9–15) (Figure 1a). A typical example of how the interplay between local and remote tertiary contacts is harnessed by the aptamer domain to generate a ligand-binding competent structure is exemplified by the adenine and guanine-sensing riboswitches (27–31). In both, the architecture of the aptamer domain is organized around a three-way junction (32), with three stem helices connected by a stretch of single-stranded nucleotides. The X-ray crystal structures available for purine riboswitches in the bound state have shown that the ligand is completely buried inside the RNA-binding pocket (26,33,34) (Figure 1b). We, and others, have shown that in the absence of the adenine ligand, Mg^{2+} ions are sufficient to promote the interaction between the P2 and P3 stem loops in the adenine riboswitch (16,17,22) (Figure 1b). This leads to an mRNA structure that is peripherally pre-organized, in a similar way to the bound-state, but with the ligand-binding pocket largely disordered (17–22). It has also been shown by chemical probing (16,35–37), nuclear magnetic resonance spectra (18,29,38,39) and thermodynamic measurements (19) that ligand binding induces a transition from this disordered 'open' state to a locally organized conformation. These results have led to the notion of ligand binding via an 'induced fit' mechanism (15,19,21,27,38,39), where the entropic cost associated to restructuring the aptamer core to accommodate the ligand is balanced by maximizing its interactions with the mRNA.

In previous studies of the *add* riboswitch aptamer from *Vibrio vulnificus* and related variants (16,17,22,40), we have shown that FRET between Cy3 and Cy5 dyes located in the loops of the P2 and P3 stems (Figure 1b) can be used to monitor the dynamics of the loop–loop interaction at the level of single-molecules. Herein, we set out to understand in further detail the dynamics and stability of the free and bound states of the add riboswitch aptamer using a single-molecule chemical denaturation approach. Although chemical denaturation is commonly used in single-molecule FRET (sm-FRET) studies of proteins (41,42) to explore their folding landscape and detect rare folding intermediates, a systematic study combining sm-FRET and chemical denaturation has never been reported for RNA or RNA-ligand complexes. On the other hand, several studies using a variety of ensemble techniques have already demonstrated how the effect of chemical-induced denaturation on large RNAs can be used to characterize the presence of kinetic traps and to provide evidence regarding the nature of the rate-limiting folding step (43–48). For instance, the folding of the P3–P7 catalytic domain of the Tetrahymena ribozyme (46) and the Bacillus subtilis RNase P (47) were both accelerated by the addition of urea, suggesting the presence of a kinetic trap along the folding pathway of these RNA structures. Understanding the nature of the rate-limiting step is even more relevant in metabolite-sensing mRNAs where the rate-limiting step might be altered by interaction of the ligand with the aptamer domain at early stages of the folding process. It is also

known that the impact of Mg^{2+} ions on the relative effect of urea can be used to characterize the nature of the rate-limiting folding step (44).

In this work, single-molecule analysis of aptamer dynamics in presence of urea as denaturant agent revealed a 50-fold decrease in the P2–P3 undocking rate of the ligand-bound state compared with the ligand-free form, in excellent agreement with values extracted from force-based mechanical unfolding (23,24). We further demonstrate that this 50-fold difference in the urea-induced unfolding rate results from unfolding events taking place from the ligand-free and ligand-bound aptamers, differing in their stability against urea denaturation. The possibility of discriminating between ligand-free and ligand-bound states purely from their dynamic properties, with no need for a conformational change between them that leads to distinctive FRET states, is a new finding afforded by the combination of sm-FRET and chemical denaturation. Lastly, we observed that while the docking rates of both, ligand-free and ligand-bound aptamers, are reduced by urea, only for the ligand-bound aptamer, the docking rate was found to strongly depend on Mg^{2+} ions. We demonstrate that these results are consistent with ligand-binding altering the rate-limiting step for tertiary folding, a feature that may be shared by other mRNA regulatory complexes. In summary, the methodology established in this work provides a novel single-molecule approach to study the dynamics of RNA and RNA-ligand complexes that will enable further investigations into how ligand sensing shapes the response of regulatory mRNAs.

MATERIALS AND METHODS

Labelling and purification of RNA oligonucleotides

Amino-modified oligonucleotides were purchased from Integrated DNA Technologies (IDT Inc.) and labelled using succinimidyl ester derivatives of Cy3 and Cy5 fluorophores following the protocol provided by the manufacturer (Invitrogen). A detailed description including nucleotide sequences is provided in the Supplementary Material. Labelled RNA strands were purified using 20% polyacrylamide gel electrophoresis containing 7 M urea and electro-eluted into 8 M ammonium acetate followed by ethanol precipitation.

Preparation of dual labelled aptamer molecules

Dual-labelled RNA aptamer molecules were prepared by T4 RNA ligation of two strands, one of them carrying the biotin and Cy3 modifications and the other carrying the Cy5 FRET acceptor. The *add* aptamer domain was assembled from oligonucleotides of the following sequences (all written in the 5′–3′ direction): 5′ STRAND: biotin- CGCCGAGCGUUGUAUAAUCCUAAUGAU AUGGUUUGGGAGU; 3′ STRAND: UUCUACCAA GAGCCUUAAACUCUUGAUUACAAACGCUCGC GC. The RNA strands were purchased from Integrated DNA Technologies Inc. with amino-modifications at the underlined positions shown in the sequences. Succinimide ester derivatives of Cy3 and Cy5 were incorporated at the specified positions followings manufacturer's protocol.

Fluorescently labelled oligonucleotides were purified as described previously (22). Purified RNA strands were annealed by heating a 1:1 mixture to 80°C in 10 mM HEPES (pH 8.0), 50 mM NaCl and slow cooling to room temperature. T4 RNA ligase (New England Biolabs) was then added to the reaction, and the sample was incubated at 37°C for 4 h. Full-length ligated RNA molecules were purified by gel electrophoresis, electroeluted and ethanol precipitated.

RNA transcription

RNA transcribed from a double-strand DNA template using T7 RNA polymerase was purified by denaturing polyacrylamide gel electrophoresis and recovered by electroelution in 8 M ammonium acetate followed by ethanol precipitation. The template for the aptamer was made from DNA oligonucleotides containing the aptamer and the T7 DNA promoter sequence. They were incubated in a 20 μM mixture containing 10 mM Tris–HCl buffer, 10 mM $MgCl_2$ and 50 mM KCl. This was then denatured by heating at 95°C for 1 min and allowed to cool down to 37°C.

2-aminopurine fluorescence binding assay

Fluorescence intensity was recorded in a Varian Cary fluorimeter. All data were collected at 20°C in 50 mM Tris–HCl buffer (pH 8.0) and 50 mM NaCl. 2-aminopurine (2AP) was excited at 300 nm, and fluorescence spectra was recorded from 310 to 450 nm. The binding affinity was obtained by monitoring the increase in fluorescence of a fixed concentration of 2AP on addition of increasing concentrations of unlabelled RNA aptamer. If the total concentration of RNA is in excess with respect to the 2AP and the stoichiometry of the RNA-ligand complex is 1:1 as suggested by the X-ray crystal structures of ligand-bound adenine complexes, the binding affinity can be described by the equation:

$$\frac{\Delta F}{F} = \frac{(1-a)[RNA]}{K_D[RNA]}$$

where ΔF is the change in fluorescence intensity, F is the fluorescence intensity in the absence of added RNA and K_D is the apparent dissociation constant. The parameter a is a dimensionless constant that represents the ratio of fluorescence quantum yield of 2AP free in solution and bound to the RNA aptamer.

Circular dichroism

Circular dichroism (CD) spectra were recorded at room temperature with a Jasco J-810 spectropolarimeter using quartz cells with a path length of 0.1 cm at an RNA concentration of 12 μM. Data were collected from 215 to 320 nm at 1 nm steps, average over four scans and smoothed for presentation.

sm-FRET

Single-molecule donor and acceptor intensity traces were acquired from single adenine aptamer molecules using a prism-based total-internal reflection microscope equipped with a 532 nm CW laser (Crystalaser, USA) and a

back-illuminated EMCCD camera (Ixon, Andor Technology, UK) mounted on an inverted microscope (Olympus IX71). Microscope slides were treated with biotinylated BSA (1 mg/ml) and neutravidin (0.2 mg/ml), and 20–200 pM dual-labelled aptamer molecules carrying a biotin group at the 5′-end were added to the slide. The imaging buffer contained 50 mM Tris–HCl (pH 8.0), 50 mM NaCl, 6% glucose (w/w), 0.02 mg/ml glucose catalase (Roche), 0.1 mg/ml glucose oxidase (Sigma), 1% 2-mercaptoethanol and the specified concentrations of $MgCl_2$ and urea. In all, 5 M urea stocks containing 6% glucose were prepared and kept in the dark. Concentrations of urea above 5 M induce a significant change in the refraction index that introduces distortions in the evanescence wave generated at the quartz-water interface. Because of this, we kept all urea concentrations at a 5 M upper limit. All measurements were performed at room temperature (20°C) using integration times of 50 and 200 ms depending on the sample dynamics. Details of the single-molecule analysis have been previously described (22).

RESULTS

Single-molecule chemical denaturation of regulatory mRNA aptamers

We previously reported that the formation of the loop–loop interaction of the adenine aptamer can be monitored using sm-FRET. For this, aptamer molecules labelled with a Cy3/Cy5 pair were immobilized on a quartz-slide via biotin-streptavidin interactions and subjected to experimental conditions (17,22,40). For reference, sm-FRET histograms obtained for the undocked and docked (with and without ligand) states, at conditions similar to those used previously to investigate the loop–loop interaction, have been included in the Supplementary section (Supplementary Figure S1). In the current work, we used a similar approach to investigate the ability of the add aptamer to undergo successive cycles of urea-based denaturation and Mg^{2+}-induced renaturation (Figure 1c). The single-molecule histogram obtained in folding buffer (4 mM Mg^{2+}, 50 mM NaCl) showed almost exclusively a single Gaussian peak centred at an apparent FRET efficiency $E_{app}\sim0.9$ (Figure 2, panel 1). As previously reported (17,22,40), this value corresponds to the Mg^{2+}-induced docked state (D) characterized by the formation of the P2–P3 loop–loop tertiary interaction. After injection of 5 M urea, while maintaining the background concentration of mono- and divalent metal ions, the single-molecule histogram shifted to an $E_{app}\sim0.3$ (Figure 2, panel 2). This low-FRET value matches that obtained in our previous studies in the absence of Mg^{2+} ions, where we demonstrated that the adenine aptamer adopts a Y-shape undocked state lacking the loop–loop interaction (UD) (22). To investigate whether the same immobilized molecules could be refolded, we next removed urea by injecting a solution containing only folding buffer. Under these conditions, the single-molecule histogram now exhibits an $E_{app}\sim0.9$ (Figure 2, panel 3), thus confirming that urea-induced denaturation is reversible and that it can be detected at the single-molecule level.
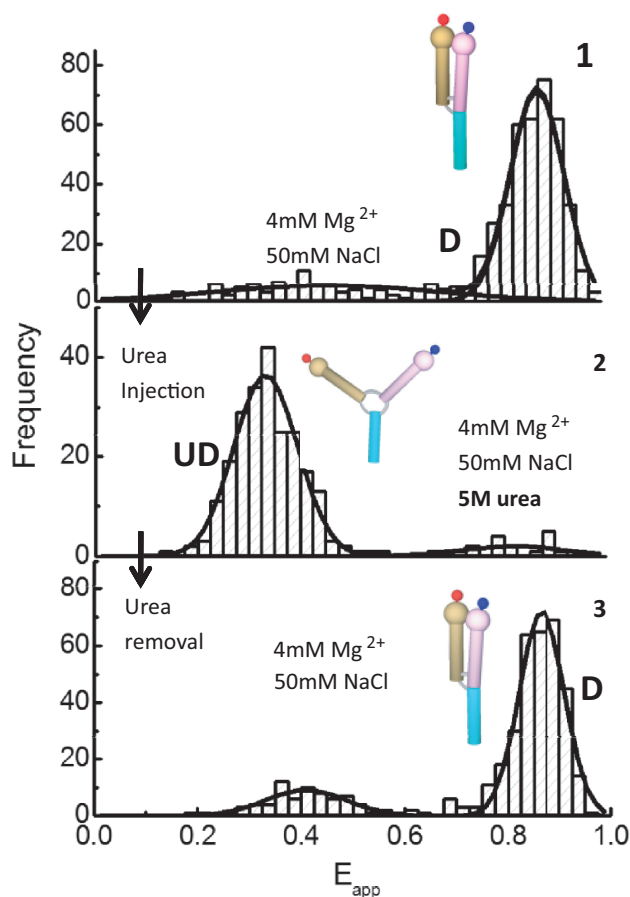

Figure 2. Single-molecule chemical denaturation of the adenine aptamer is reversible and specific to the tertiary structure. Single-molecule histograms at 4 mM Mg^{2+} and 50 mM NaCl (panel 1) showed most of the aptamer molecules in the docked conformation (D). In this state, the formation of the loop–loop interaction brings the donor in close proximity to the acceptor resulting in a high FRET state ($E_{app}\sim0.9$). Injection of urea to the same surface-immobilized aptamers (panel 2), while maintaining the concentration of mono- and divalent metal ions, shifted the single-molecule histogram to a low FRET state ($E_{app}\sim0.45$) corresponding to the undocked state (UD). An additional cycle of urea removal shifted back the single-molecule histogram to the high FRET docked state (panel 3).

To confirm that under our experimental conditions, urea-induced denaturation of the adenine aptamer is restricted to its tertiary structure, we performed CD spectroscopy. In the absence of urea, the docked state of the adenine aptamer obtained at 4 mM Mg^{2+} showed a large positive ellipticity with a maximum at 265 nm that decreased slightly (~10%) on addition of 5 M urea. Small variations in this band have been observed for other three-way RNA junctions (49) as a function of metal ions and have been taken as evidence for tertiary folding/unfolding processes. Importantly, the CD spectra registered in the absence of metal ions, which can be assigned to the undocked tertiary structure, is very similar to that obtained at 5 M urea in a background of 4 mM Mg^{2+} (Supplementary Figure S2). This suggests that the RNA exhibits a very similar tertiary structure under both experimental conditions. In contrast, the CD spectra obtained at 7 M urea in the absence of metal ions showed

a very significant decrease in the intensity at 265 nm ($\sim$57%) and a concomitant shift to a slightly higher wavelength ($\sim$5 nm) (Supplementary Figure S2). These variations in the CD spectra are characteristic of large-scale disruptions in base stacking and have been interpreted as indicative of secondary structure denaturation of the RNA (49,50). In fact, the CD spectra obtained for the adenine aptamer at 7 M urea agrees remarkably well with those reported under heat-induced and cold-denaturing conditions for the hammerhead ribozyme (51), a structurally related three-way RNA junction. From this data, we concluded that the secondary structure of the adenine aptamer is maintained under the experimental conditions used to promote urea-induced undocking. Notably, no change in the density of immobilized aptamers was observed at high urea, suggesting no significant disruption of the neutravidin-biotin interactions used for RNA immobilization. This is in agreement with the observed stability of the neutravidin tetramer, both in the apo- and biotin-bound forms, even at denaturant concentrations above 6 M urea (52).

Urea-induced undocking of ligand-free aptamers

From a regulatory perspective, ligand-free and ligand-bound states of metabolite-sensing mRNAs are equally important, as each of them is responsible for one of the two possible outcomes of the gene regulation process (9–12,15). Given that P2–P3 loop–loop interaction has previously been reported to be crucial for riboswitch function (17,18,22), we started our analysis by exploring the effect that chemical denaturation has on the P2–P3 loop dynamics and equilibrium populations of the unliganded state. To ensure that RNA aptamers are in the docked state before the addition of urea, we carried out our assays at a fixed 4 mM concentration of Mg^{2+} ions. On increasing the denaturant concentration, we observed a progressive decrease in the relative contribution of the docked state D ($E_{app}\sim$0.9) and a concomitant increase in the contribution of a Gaussian peak at a lower FRET (Figure 3a). This low-FRET state gradually shifts from an $E_{app}\sim$0.45 without urea to an $E_{app}\sim$0.25 at 5 M urea, the latter corresponding to the undocked state UD. We previously observed a similar shift from $E_{app}\sim$0.25 to
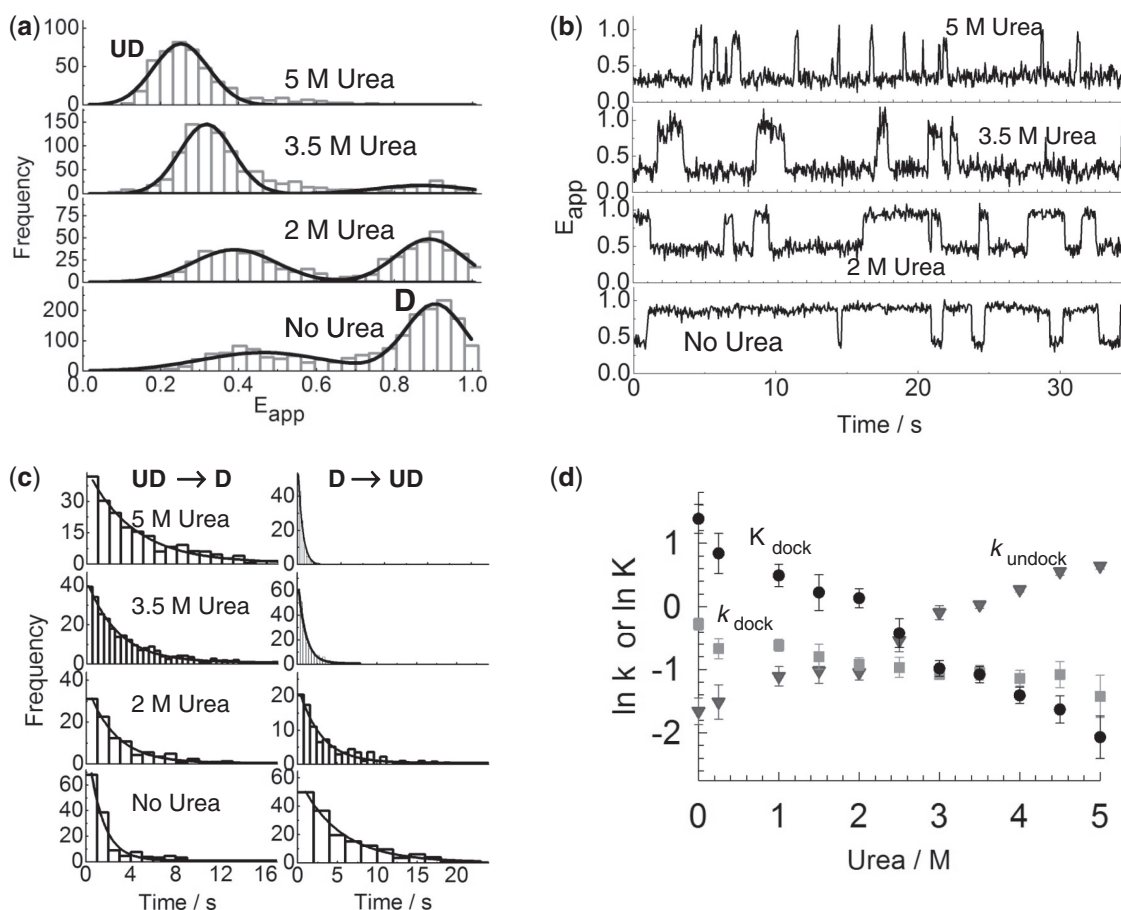

Figure 3. Urea-induced undocking of ligand-free adenine aptamers. (**a**) Single-molecule histograms of FRET efficiency as a function of urea concentration. All histograms have been obtained in a background of 4 mM Mg^{2+} and 50 mM Na^+ ions. (**b**) sm-FRET trajectories obtained with 50 ms integration time at the indicated concentrations of urea. (**c**) Single-molecule dwell-time histograms of the UD (left panels) and D (right panels) states at the indicated urea concentrations. The data have been fitted to single exponential functions to extract the docking (k_{dock}) and undocking (k_{undock}) rates, respectively. (**d**) Effect of urea on the equilibrium constant (K_{dock}) and docking (k_{dock}) and undocking (k_{undock}) kinetics of ligand-free aptamers at 4 mM concentration of Mg^{2+} ions.

$E_{app} \sim 0.5$ when analysing the Mg^{2+}-induced folding pathway (22), and we found that docking of the P2–P3 stems takes place via an intermediate structure characterized by an $E_{app} \sim 0.5$. Remarkably, the shift in the low-FRET peak observed with urea is identical to that taking place during Mg^{2+}-induced docking. This suggests that urea promotes an undocking pathway very similar to the folding landscape of the add aptamer in Mg^{2+} ions. As the urea concentration is increased, transitions between the D and UD states become more frequent with the aptamer progressively remaining in the UD state for longer periods (Figure 3b). Above 3.5 M urea, the aptamer is almost exclusively in the undocked state with occasional short transitions to the docked conformation. From these trajectories, we obtained the single-molecule dwell time histograms for the UD and D states at each urea concentration (Figure 3c). It is clear that urea has an opposite effect on docking and undocking rates, progressively slowing down the docking process whilst strongly accelerating undocking. However, the degree of dynamic heterogeneity remained comparable with that obtained in the absence of urea (<10-fold) and constant across the entire range of urea concentrations, thus ruling out the presence of urea as a source of dynamic heterogeneity in the ligand-free state (Supplementary Figure S3). We fitted the single-molecule dwell-time histograms to single exponential decay functions to extract the docking (k_{dock}) and undocking (k_{undock}) rates (Figure 3d, Supplementary Table S1), respectively. Although the addition of 5 M urea was found to moderately decrease k_{dock} from $0.71 \pm 0.07 \, s^{-1}$ to $0.24 \pm 0.1 \, s^{-1}$, k_{undock} was strongly increased by 10-fold from $0.19 \pm 0.04 \, s^{-1}$ to $1.9 \pm 0.1 \, s^{-1}$. The equilibrium constant (K_{dock}) calculated from the k_{dock} and k_{undock} values was reduced by 30-fold between 0 and 5 M urea (Figure 3d). These findings suggest that the interaction between urea and the ligand-free mRNA aptamer reduces its docking equilibrium, and that this effect results from a substantial increase of k_{undock} accompanied by a moderate decrease in k_{dock}.

Rate-limiting step for ligand-free docking

To investigate the precise nature of the rate-limiting step for docking of the ligand-free aptamer, we investigated the relative effect of urea across a 40-fold variation in the concentration of Mg^{2+} ions. For clarity, only results obtained at sub-saturating (0.1 mM) and saturating (2 mM) Mg^{2+} ions in the presence and absence of 2M urea are shown (Figure 4). The sm-FRET and dwell-time histograms along with the calculated kinetic rates and equilibrium constants for all Mg^{2+} and urea concentrations studied are shown in the Supplementary Data (Supplementary Figures S4 and S5 and Supplementary Tables S2–S4). We fitted the single-molecule dwell-time histograms obtained at 0.1 mM Mg^{2+} (Figure 4a) and
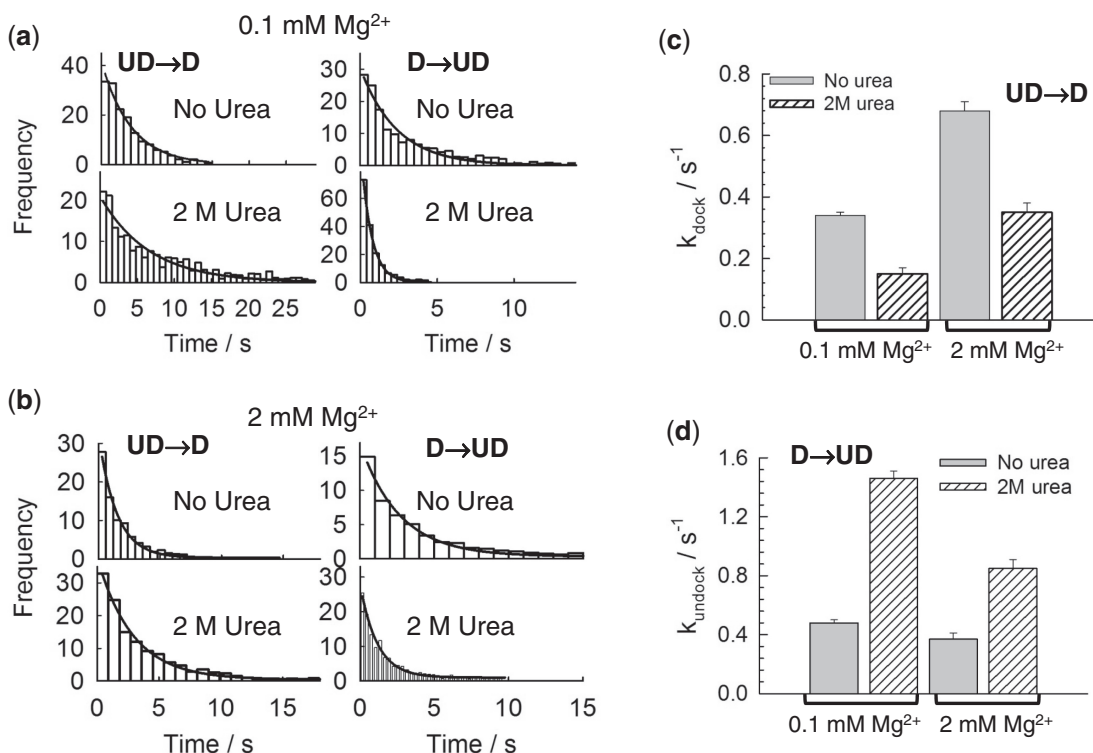

Figure 4. Docking and undocking dynamics of ligand-free aptamers as a function of Mg^{2+} ions in the presence and absence of urea. (**a** and **b**) Single-molecule dwell-time histograms at 0.1 mM Mg^{2+} (**a**) and 2 mM Mg^{2+} (**b**) obtained for the docking (left panels) and undocking (right panels) processes in the absence (grey) and presence (pattern) of 2M urea concentration. The data have been fitted to single exponential decay functions to extract the docking (k_{dock}) and undocking (k_{undock}) rate constants, respectively. (**c** and **d**) Values of k_{dock} (**c**) and k_{undock} (**d**) obtained in the absence (grey) and presence of 2M urea (pattern) at sub-saturating (0.1 mM) and saturating (2 mM) concentrations of Mg^{2+} ions.

2 mM Mg^{2+} (Figure 4b) to a mono-exponential decay function. The k_{dock} had values of $0.25 \pm 0.01\,s^{-1}$ at 0.1 mM Mg^{2+} and $0.65 \pm 0.02\,s^{-1}$ at 2 mM Mg^{2+} in the absence of urea, and is approximately halved to values of $0.15 \pm 0.01\,s^{-1}$ and $0.33 \pm 0.02\,s^{-1}$ on addition of 2 M urea (Figure 4c). Urea-induced deceleration of the docking rate was also reported for the two-way hairpin ribozyme (48), which shows a docking rate ($2.5\,s^{-1}$) similar to that of the ligand-free adenine aptamer ($0.8\,s^{-1}$) at saturating concentrations of Mg^{2+} ions. For k_{undock}, the effect of 2 M urea was slightly higher at 0.1 mM Mg^{2+} than at 2 mM Mg^{2+}, increasing by 3- and 2-fold, respectively (Figure 4d). The fact that the relative magnitude of urea-induced deceleration observed for k_{dock} is practically constant across all Mg^{2+} concentrations explored (Figure 4c and Supplementary Figure S6) strongly supports a trap-free conformational search mechanism as the rate-limiting step in the docking pathway of the ligand-free aptamer as discussed later in more detail.

RNA-ligand interactions stabilize the bound state against urea-induced undocking

Ligand-induced stabilization of the aptamer domain is at the heart of the gene-regulation process. In this context, we reasoned that urea acting as a driving force to disrupt the mRNA-ligand complex could provide valuable insights into the relative stability of ligand-free and ligand-bound aptamers. To evaluate this, we performed a sm-FRET investigation of the adenine aptamer in the presence of adenine ligand (100 µM) at increasing concentrations of urea (Figure 5a). We observed a progressive increase in the relative population of the UD state reaching a value of 64% at 5 M urea (Figure 5a). This value is considerably lower than in the absence of ligand, where a similar concentration of urea promoted an almost complete shift towards the UD state (Figure 3a). These results indicate that the formation of the RNA-ligand complex strongly protects the docked state from urea-induced undocking. The sm-FRET trajectories showed a higher frequency of fluctuations between the D and UD states, as the concentration of urea was increased (Figure 5b) with the dwell times of the docked state at 5 M urea being more than order of magnitude longer than in the absence of ligand (Figure 3b). Although 100 µM concentration of adenine ligand provides a suitable dynamic range to analyse the competing effects of ligand and denaturant on the stability of the D state, the fact that 64% of aptamers remained undocked (Figure 5a, top panel) clearly indicates that 100 µM is not enough ligand concentration to completely counteract the undocking effect of
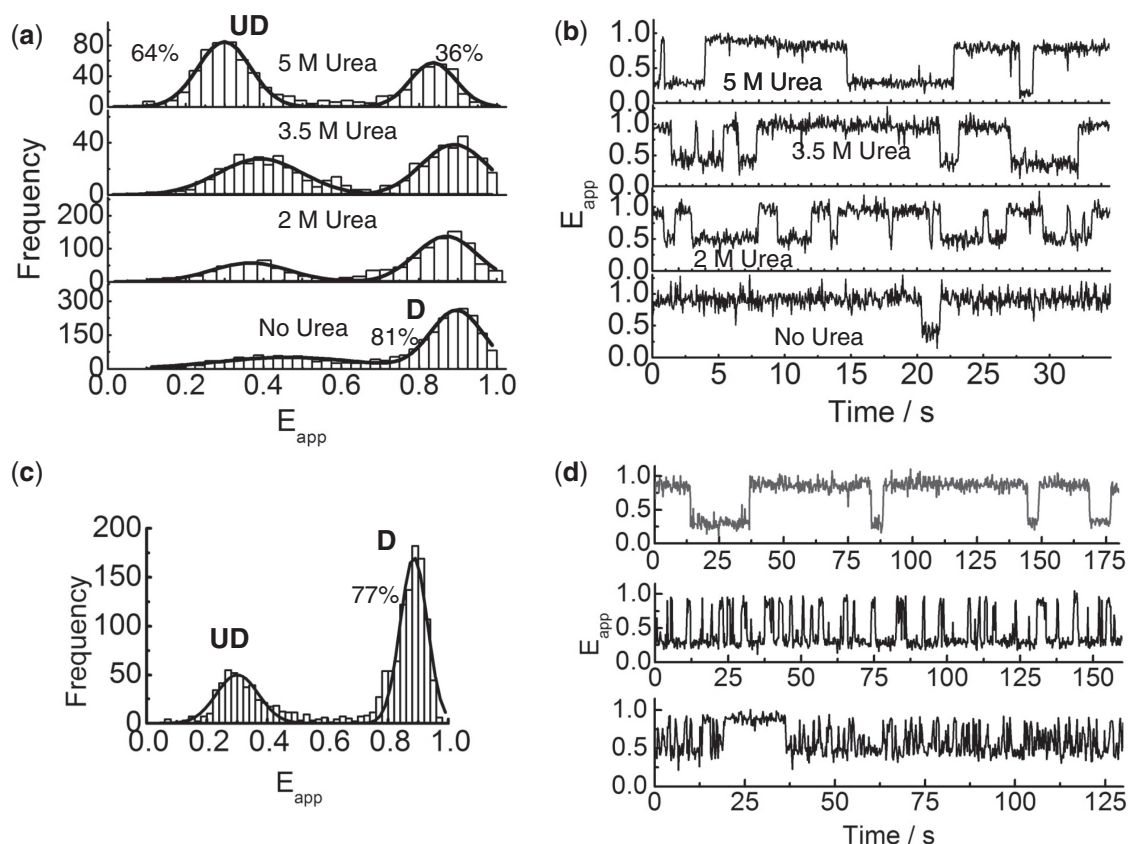

Figure 5. Urea-induced undocking of ligand-bound adenine aptamers. (**a**) sm-FRET histograms obtained at the indicated concentrations of urea in a background of 4 mM Mg^{2+} ions and 100 µM adenine ligand. (**b**) Representative sm-FRET trajectories as a function of increasing urea concentration in the presence of 100 µM adenine and 4 mM concentration of Mg^{2+} ions. (**c**) sm-FRET histogram obtained in the presence of 5 M urea and 500 µM adenine ligand. (**d**) Representative sm-FRET trajectories obtained in a background of 4 mM Mg^{2+} ions and in the presence of 5 M urea and 500 µM adenine ligand.

5 M urea. Because 5 M urea completely shifted the ligand-free aptamer towards the UD state (Figure. 3a), and to compare this equilibrium population with that at saturating concentrations of metabolite, we obtained the single-molecule histogram at 5 M urea using a 5-fold higher concentration of adenine ligand (Figure 5c). Under these conditions, the aptamer remained mostly on the D state and showed a heterogeneous dynamic behaviour. The majority of traces (Figure 5d, Supplementary Figure S7) showed an extremely long-lived D state lasting for several tens of seconds (Figure 5d, top panel). However, 20% of them exhibited a very rapid interconversion dynamics between short-lived D and UD states (Figure 4d, middle panel), and a remaining 3% of

the traces displayed a combination of short- and long-lived D states (Figure 5d, bottom panel).

Dynamics-based sorting of ligand-free and ligand-bound states

To investigate further the observed dynamic heterogeneity described earlier in the text, single aptamers were titrated with increasing amounts of ligand at constant concentrations of 4 M urea and 4 mM Mg^{2+} ions. The relative population of UD progressively decreased from ~80% in the absence of ligand to ~55% at 100 μM ligand concentration (Figure 6a). The sm-FRET trajectories displayed clear transitions between both states, and their relative dwell times exhibited a strong dependence on ligand
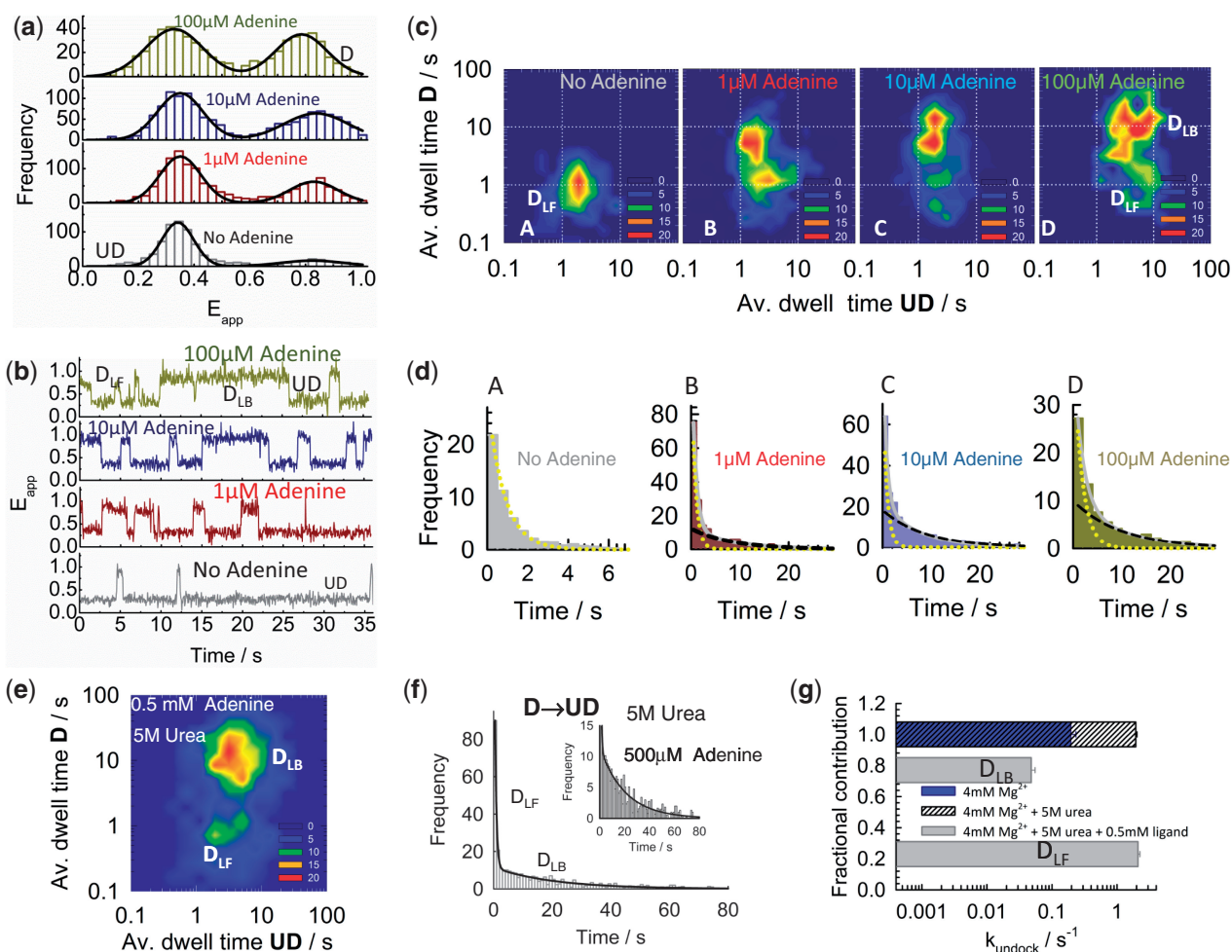

Figure 6. Relative stability and dynamics of coexisting undocked (UD), ligand-free (D_{LF}) and ligand-bound (D_{LB}) docked states.(a) Single-molecule histograms of FRET efficiency in the presence of 4 M urea and 4 mM Mg^{2+} showing the variation in the relative populations of the docked D and UD states as a function of ligand concentration. (b) Examples of sm-FRET trajectories obtained at the specified concentrations of adenine ligand in the presence of 4 M urea and 4 mM Mg^{2+}. (c) 2D contour plots of the average dwell times on the D and UD states obtained from the analysis of >400 molecules at the indicated concentrations of adenine ligand.(d) Single-molecule dwell-time histograms of undocking events as a function of increasing adenine ligand concentration. The decay has been fitted to mono- (no ligand) and bi-exponential functions (with ligand). Dotted lines represent the relative contribution to the biexponential decay from undocking events taking place from the short-lived D_{LF} state. Dashed lines represent the relative contribution from undocking events taking place from the long-lived ligand-bound state (D_{LB}). (e) Two-dimensional contour plot showing the distribution of average docking and undocking dwell times at 4 mM Mg^{2+}, in the presence of 5 M urea and 500 μM adenine ligand. (f) Solid line represents the non-linear squares fitting to a bi-exponential decay function. From the fitting, we obtained values of rate constants $2.1 \pm 0.1 \, s^{-1}$ (minor component) and $0.045 \pm 0.003 \, s^{-1}$ (major component). (g) Variation in the undocking rates on addition of saturating concentrations of urea and adenine ligand.

concentration (Figure 6b). As the concentration of adenine increased, we observed a progressive switch from relatively short-lived D states (<2 s) to D states lasting $\sim$10–20 s. To quantify the observed switching behaviour, we generated two-dimensional contour plots of the average residence times of single aptamer molecules in each state (D and UD) as a function of ligand concentration (Figure 6c). In the absence of ligand, the average residence time in both states displayed very little dynamic heterogeneity (Figure 6c, panel A). In contrast , as the concentration of ligand increased, the average residence time in the D state progressively shifted to longer values (Figure 6c, panels B–D), spanning more than two orders of magnitude at 100 µM ligand concentration. To evaluate k_{undock} as a function of ligand concentration, we calculated the dwell-time histograms for the D state (Figure 6d, panels A–D). With ligand added, they exhibited a bi-exponential decay (Figure 6d, panels B–D). The fast component showed an identical rate to that obtained in the absence of ligand ($\sim$1.2 $\pm$ 0.01 s^{-1}) (Figure 6d, panel A), whereas the slow component exhibited a value that was $\sim$10-fold slower ($\sim$0.14 $\pm$ 0.01 s^{-1}). Therefore, the fast and the slow components of the biexponential decay must correspond to undocking events taking place from the ligand-free (D_{LF}) and the ligand-bound state (D_{LB}), respectively. This assignation is further supported by the change in the associated pre-exponential factors as a function of ligand concentration (Supplementary Table S5).

Ligand-induced 'locking' of the aptamer domain in its bound state is intrinsic to the gene regulation mechanism of many mRNAs (12,15,26). Thus, the dynamics-based differentiation of ligand-free and ligand-bound states developed here has the potential to characterize the functional dynamics in a variety of regulatory complexes without the requirement for a structural change associated to ligand binding. Here, we have used this property to quantify the ligand-induced stabilization of the docked state. For this, we required conditions where the D_{LB} state is substantially populated, and at the same time, there is enough concentration of denaturant agent to significantly induce undocking events. A 2D average dwell-time contour plot generated at 5 M urea and 500 µM ligand showed two well-defined classes of undocking rates with average values differing more than 10-fold (Figure 6e). Moreover, the majority of the molecules showed long-lived residence times in the docked state characteristic of the ligand-bound state, thus confirming the $D_{LB}{\rightarrow}$UD route as the predominant undocking pathway (Figure 6d). Single-molecule dwell-time histograms displayed an initial fast component followed by a very slow decay with fractional contributions of 0.16 $\pm$ 0.04 and 0.84 $\pm$ 0.01, respectively (Figure 6f). As before, we assigned the minor component to urea-induced D_{LF} undocking with a decay rate (2.1 $\pm$ 0.1 s^{-1}) that is in perfect agreement with that obtained in the absence of ligand (1.94 $\pm$ 0.01 s^{-1}) (Figure 3c). By comparing the relative magnitude of the undocking rates, with (0.045 $\pm$ 0.003 s^{-1}) and without ligand (2.1 $\pm$ 0.1 s^{-1}) (Figure 6g), we estimated a $\sim$50-fold stabilization of the D_{LB} versus the D_{LF} state. This is in very good agreement

with the two orders of magnitude stabilization recently observed using optical tweezers (25).

Ligand binding alters the rate-limiting step for docking

It has been shown that ligand binding can take place at sub-saturating concentrations of divalent metal ions, where loop–loop tertiary interactions are only transiently formed (17–19). In this context, it is interesting to investigate whether ligand binding at an early stage of the folding process may alter the rate-limiting step for docking. To address this, we have performed a comparative analysis of the effect of urea on the docking rates as a function of Mg^{2+} and ligand concentration. At concentrations of Mg^{2+} ions below saturation (100 µM) and in the presence of 100 µM concentration of adenine ligand, the sm-FRET histogram (Figure 7a, left top panel) showed the majority of aptamer molecules located in the D state ($\sim$60%), and the corresponding FRET trajectories (Figure 7a, left bottom panel, Supplementary Figure S8a) displayed fast fluctuations between D and UD states. On addition of 2 M urea, the sm-FRET histogram (Figure 7b, right top panel) indicated a substantial shift towards the UD state (77%). Inspection of the anti-correlated donor and acceptor traces and the corresponding FRET trajectories revealed a remarkably slower k_{dock} in presence of 2 M urea (Figure 7a, right bottom panel, Supplementary Figure S8b).

To evaluate whether this effect on k_{dock} could depend on the concentration of Mg^{2+} ions, we obtained the single-molecule dwell time histograms for the D state at 100 µM (Figure 7b, left panels) and 4 mM (Figure 7b , right panels) concentration of Mg^{2+} ions, with (Figure 7b, bottom panels) and without urea (Figure 7b, top panels). At 4 mM concentration of Mg^{2+} ions, addition of 2 M urea decreased the rate constant from 0.71 $\pm$ 0.04 s^{-1} to 0.31 $\pm$ 0.03 s^{-1} (Figure 7b, right panels). This $\sim$2-fold reduction in the docking rate constant is almost identical to that obtained in the absence of adenine ligand (Supplementary Table S1 and Supplementary Figure S9). In contrast, at 100 µM concentration of Mg^{2+} ions, k_{dock} changed by $\sim$8-fold from 0.49 $\pm$ 0.02 s^{-1} with no urea to 0.061 $\pm$ 0.003 s^{-1} at 2 M urea (Figure 7b, left panels). The effect of urea in k_{dock} deceleration in the presence of ligand was further confirmed by the 2D contour plots generated at similar experimental conditions (Supplementary Figure S10). Because it is known that ligand binding moderately accelerates docking (16–19,53,54) and to determine whether a significant urea-induced change in ligand binding affinity could account for the observed decrease in k_{dock}, we calculated the dissociation constant in the absence and presence of 2 M urea using a 2AP fluorescence assay in which 2AP replaced the adenine ligand to report the formation of the aptamer-ligand complex (22). The normalized variation in 2AP fluorescence intensity was fitted to a simple two-state binding model with no cooperativity, and dissociation constants of 4.1 $\pm$ 0.5 µM in the absence of urea and 10 $\pm$ 2 µM in the presence of 2 M concentration of urea were obtained (Figure 7c). This relatively small variation ($\sim$2.5-fold) in ligand binding
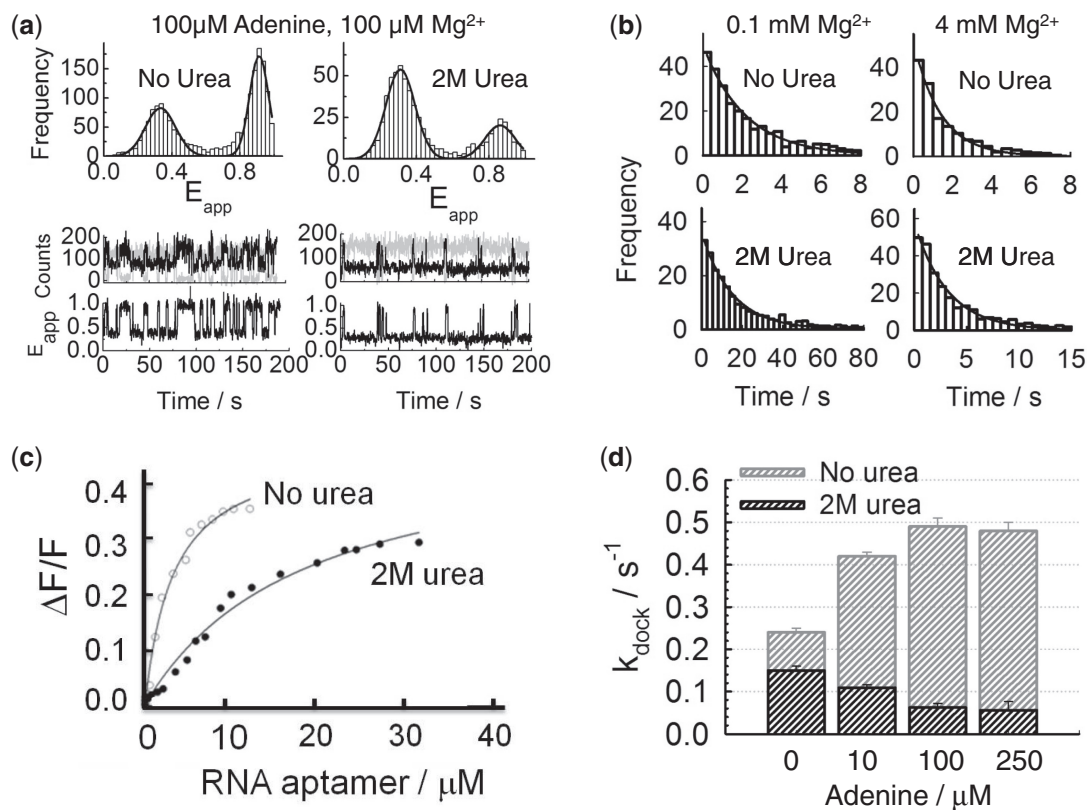
Figure 7. Urea-induced deceleration of ligand-bound docking is highly dependent on Mg^{2+} ions. (**a**) sm-FRET histograms (upper panels) and representative anti-correlated donor-acceptor and FRET trajectories (bottom panels) obtained at sub-saturating concentrations of Mg^{2+} ions (100 μM) in the absence (left panel) and presence (right panel) of 2 M urea. (**b**) Single-molecule dwell-time histograms obtained for the docking process in a background of 100 μM adenine ligand at 100 μM (left panels) and 4 mM (right panels) concentration of Mg^{2+} ions. Results are shown in the absence (top panels) and presence of 2 M urea (bottom panels). (**c**) Normalized 2AP fluorescence intensity plotted as a function of adenine aptamer concentration obtained at 100 μM Mg^{2+} in the absence (○) and presence of 2 M urea (●). Changes in fluorescence (ΔF) were normalized to the maximum fluorescence measured in the absence of RNA (F). The line shows the best fit to a simple binding model (see 'Materials and Methods' section) yielding values of 4.1 ± 0.5 μM Mg^{2+} and 10 ± 2 μM Mg^{2+}, respectively. (**d**) Comparison of k_{dock} (s^{-1}) values as a function of ligand concentration in the absence and presence of 2 M urea. All values have been obtained at 100 μM constant concentration of Mg^{2+} ions.

affinity induced by urea clearly indicates that the observed decrease in k_{dock} is not, at least entirely, caused by the disruption of ligand binding by competing urea.

To get further insights into the observed role of ligand binding modulating the docking dynamics at sub-saturating Mg^{2+} concentrations, we investigated the relative changes in k_{dock} as a function of ligand concentration (Supplementary Figure S11). At 100 μM concentration of Mg^{2+} ions and in the absence of urea, increasing the ligand concentration induced a ~2-fold acceleration of the docking rate (Figure 7d). This effect is in agreement with previous studies of the docking process (22) and confirms that the ligand can act as a folding enhancer by interacting with open loop–loop conformations of the aptamer domain and subsequently driving the aptamer towards the native state. In the presence of 2 M urea, the dependence of k_{dock} with the concentration of adenine is remarkably different. As the ligand concentration was progressively increased, k_{dock} changed from ~$0.15 \pm 0.01\,s^{-1}$ in the absence of ligand to a value of ~$0.05 \pm 0.02\,s^{-1}$ at 250 μM ligand concentration (Figure 7d, Supplementary Table S6). This represents a relative decrease in k_{dock}, with respect to the values obtained in the absence of urea

of ~1.6- and ~8.5-fold, respectively. Thus, in the presence of ligand, a urea-induced deceleration of the docking rate being significantly more pronounced at sub-saturating Mg^{2+} ions, whilst having a moderate effect at high Mg^{2+} concentrations, is consistent with a rate-limiting step that requires the consolidation of the RNA structure around one or more specific metal ion binding sites (44), as those observed in the crystal structure of the adenine aptamer (20).

DISCUSSION

We have used a combination of sm-FRET and urea-induced tertiary denaturation to compare the loop–loop docking dynamics and the relative stability of the free and ligand-bound forms of the add riboswitch sensing domain. Our single-molecule denaturation experiments reveal two distinct effects induced by ligand binding. First, higher concentrations of urea are required in the presence of ligand to induce a similar shift in the relative equilibrium populations of the docked (D) and undocked (UD) states to that observed for the ligand-free form (Figures 3a and 5a). Second, increasing the ligand concentration at

constant urea induces a pronounced increase in the degree of dynamic heterogeneity associated to the undocking process (Figure 5 and 6). The observed dependence of both effects with the concentration of adenine ligand clearly indicates that they are caused by the formation of the aptamer-ligand complex and the subsequent protection of the ligand-bound state against denaturation.

Remarkably, the biexponential decay obtained for the urea-induced undocking process in the presence of adenine ligand (Figure 6d) demonstrates, for the first time, the potential of single-molecule chemical denaturation to distinguish, within the same mRNA, coexisting undocking events taking place from the ligand-free (D_{LF}) and the ligand-bound (D_{LB}) states. Here, we used this difference in k_{undock} to determine a $\sim$50-fold stabilization of D_{LB} relative to D_{LF} owing to ligand binding (Figure 5g).We hypothesize that discriminating between D_{LB} and D_{LF} states using their different stability and undocking dynamics against urea denaturation might become particularly useful when investigating other artificial and naturally occurring RNA-ligand complexes for which ligand binding does not induce additional changes in inter-dye distance. SAM-I (55), SAM-II (56), aminoglycoside-binding riboswitches (57) and the glms ribozyme (58) are some recent examples of such mRNA complexes, where the formation of the native state involves a conformational capture mechanism that alters the equilibrium populations of pre-existing RNA conformers without affecting the global architecture of the mRNA.

Although the exact nature of the interactions between the RNA and urea are still not entirely understood (44, 59), acceleration of RNA folding by urea is emerging as a signature of kinetic traps as the rate-limiting step in large RNAs (47). Among potential sources of kinetic traps in the add aptamer, the formation of anomalous P1–P2 helical stacking conformers and non-native nucleotide interactions within the aptamer core are obvious candidates. If the formation of these or other misfolded states constitutes a kinetic barrier, urea should accelerate folding. In contrast, k_{dock} decreases with increasing urea concentrations at all concentrations of Mg^{2+} ions and adenine ligand investigated, suggesting a trap-free rate-limiting step. In turn, a trap-free docking pathway additionally reinforces the transient-state previously reported by sm-FRET as an on-path partially folded intermediate structure (22,60). A model describing the observed ligand-induced switching in the rate-limiting step for docking is illustrated in Figure 8. In the absence of ligand, the similar level of k_{dock} deceleration observed across a 40-fold variation in the concentration of Mg^{2+} ions (Figure 4c and Supplementary Figure S6) indicates a conformational search mechanism as the rate-limiting step for loop–loop docking (Figure 8). The molecular basis of the key tertiary contacts involved in the aptamer conformational search will be the subject of additional investigations. Nevertheless, given that the aptamer core has been shown to remain largely unstructured in the absence of ligand (16–22), it is tempting to speculate that most likely, it will involve interactions between peripheral elements of the aptamer domain. In this context, the
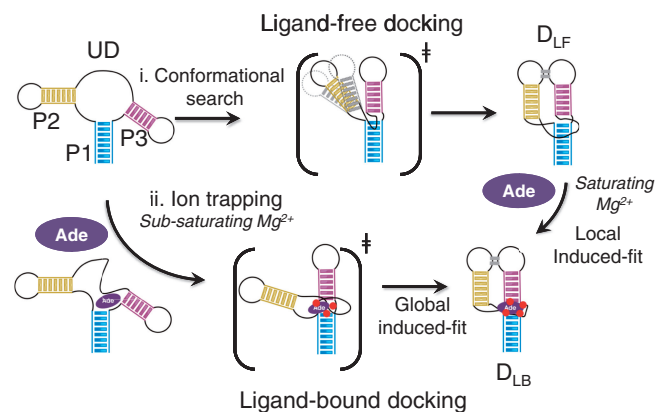

Figure 8. Ligand-induced switching of the rate-limiting step for aptamer docking. (i) In the absence of ligand, the rate-limiting step for stabilization of the ligand-free docked state (D_{LF}) involves the formation of key tertiary contacts between the undocked (UD) P2 and P3 stem loops (conformational search model). (ii) Ligand binding to partially folded or unfolded aptamer domains induces a switch to a rate-limiting step involving the consolidation of the ligand-aptamer complex (D_{LB}) around specifically captured Mg^{2+} ions (ion trapping model) as those observed in the X-ray structure. Red spheres represent specifically bound Mg^{2+} ions, and their number and location within the aptamer core is shown only for illustrative purposes.

stability of the apical base pairs in helix P2 has been suggested to be crucial for the formation of a productive and stable loop–loop interaction (18,28). Indeed, a A30G/U40C mutant of the pbuE adenine aptamer in which the weaker A:U interaction was replaced by the more stable G:C base pair showed the formation of the P2–P3 loop–loop interaction even in the absence of Mg^{2+} ions (18). A rate-limiting step based on the formation of specific tertiary contacts between two internal loops present in adjacent helical motifs has also been proposed for the minimal hairpin ribozyme (48).These analogies suggest that productive encounters between peripheral folding elements and subsequent rearrangement of their secondary structure may be a widespread feature contributing to the folding free-energy barrier of other functional RNAs.

In the presence of adenine ligand, urea also decreases k_{dock}. However, in contrast to what we observed for the ligand-free state, its deceleration effect on k_{dock} is strongly sensitive to the concentration of Mg^{2+} ions. This sensitivity in k_{dock} suggests a different rate-limiting step for docking in which Mg^{2+} ions are essential to achieve the ligand-bound native state (Figure 8). The molecular basis of such ligand-induced switching in the rate-limiting step can be justified based on the observation of productive ligand binding in partially unfolded aptamers or even in those with disrupted loop–loop interactions (19,35). We and others have shown that the ligand-bound state of adenine and guanine riboswitches adopts a single conformation at saturating concentrations of Mg^{2+} ions (22.39) (>2 mM). However, when docking is compromised, e.g. at low concentrations of Mg^{2+} ions, ligand binding may not be sufficient to dock the aptamer structure, leading to an array of coexisting and partially docked ligand-bound states that differ in local and global tertiary structure as recently suggested by stopped-flow (54), sm-FRET (22) and ultra-fast time-resolved spectroscopy (36,37). In this context,

funneling this ensemble of stiff-liganded states towards a tightly packed mRNA-ligand complex, resembling the X-ray structure (20), may require assistance from specifically trapped divalent metal ions along the docking pathway. Indeed, the crystal structure of the liganded add aptamer domain shows up to five Mg^{2+} ions, two of them placed near the binding pocket (20). Based on this, we reasoned that a transition state involving the formation of one or more Mg^{2+} ion-binding sites may reflect the need to counteract the increase in negative charge density owing to backbone phosphate oxygens brought in close proximity ($\sim$3.6 Å) around the bound ligand (20). In fact, a recent thermodynamic investigation on the effect of Mg^{2+} on the add free energy folding landscape also suggested that Mg^{2+} binding to undocked loops strongly decreases the energetic cost involved in reorganizing the binding pocket to accommodate the ligand (19). The importance of two penta-hydrated Mg^{2+} ions anchoring the junction proximal ends of helices P2 and P3 for ligand recognition has also been suggested by molecular dynamics simulations (21).

A ligand-induced switching on the rate-liming step sheds new light into how the formation of the mRNA-ligand complex drives the sensor domain towards the ligand-bound native state. Taken together, our data are fully consistent with an 'induced-fit' folding model (Figure 8). However, the extent of the conformational rearrangements taking place depends on whether the ligand associates to a fully folded docked state (D_{LF}) or to partially folded aptamers (UD). In the first scenario, at saturating Mg^{2+} ions, changes leading to the D_{LB} state are locally restricted to the aptamer core (local or predetermined induced fit). On the other hand, at sub-saturating Mg^{2+} ions, compaction of the RNA around the bound ligand to form the D_{LB} complex is mediated by specifically trapped Mg^{2+} ions and involves the formation of long-range tertiary contacts in addition to the local network of interactions that stabilize the aptamer core (global induced-fit). Although further investigations are needed to determine which and how many of the Mg^{2+} ions present in the high resolution structure may actively participate in docking and ligand binding, our work provide evidences for a strong link between metabolite sensing, localized Mg^{2+} binding and tertiary folding that may be common to other mRNA-ligand regulatory complexes for which the X-ray structure has shown the presence of specifically bound divalent metal ions (61,62). In conclusion, we have demonstrated that the competing interplay of Mg^{2+} ions and chemical denaturation is a useful tool to investigate RNA functional dynamics at single-molecule level. Modulating such interplay within single RNAs and RNA-ligand complexes to isolate and further characterize transient intermediate and low-populated states may be possible using single-molecule chemical denaturation.

SUPPLEMENTARY DATA

Supplementary Data are available at NAR Online: Supplementary Tables 1–6 and Supplementary Figures 1–11.

REFERENCES

1. Joo,C., Balci,H., Ishitsuka,Y., Buranachai,C. and Ha,T. (2008) Advances in single-molecule fluorescence methods for molecular biology. *Ann. Rev. Biochem.*, **77**, 51–76.
2. Tinoco,I. Jr and Gonzalez,R.L. Jr (2011) Biological mechanisms, one at a time. *Genes Dev.*, **25**, 1205–1231.
3. Nienhaus,G.U. (2009) Single-molecule fluorescence studies of protein folding. *Methods Mol. Biol.*, **490**, 311–337.
4. Schuler,B. and Eaton,W.A. (2008) Protein-folding studied by single-molecule FRET. *Curr. Opin. Struct. Biol.*, **18**, 16–26.
5. Zhuang,X. (2005) Single-molecule RNA science. *Ann. Rev. Biophys. Biomol. Struct.*, **34**, 399–414.
6. Bokinsky,G. and Zhuang,X. (2005) Single-molecule RNA folding. *Acc. Chem. Res.*, **38**, 566–573.
7. Sosnick,T.R. (2001) Characterization of tertiary folding of RNA by circular dichroism and urea. *Curr. Protoc. Nucleic Acid Chem.*, **4**, 115.1–11.5.10.
8. Theimer,C.A. and Giedroc,D.P. (1999) Equilibrium unfolding of an H-type RNA pseudoknot which promotes programmed -1 ribosomal frameshifting. *J. Mol. Biol.*, **289**, 1283–1299.
9. Roth,A. and Breaker,R.R. (2009) The structural and functional diversity of metabolite-binding riboswitches. *Annu. Rev. Biochem.*, **78**, 305–334.
10. Serganov,A. and Patel,D.J. (2012) Metabolite recognition principles and molecular mechanism underlying riboswtich function. *Ann. Rev. Biophys.*, **4**, 343–370.
11. Lemay,J.F., Desnoyers,G., Blouin,S., Heppell,B., Bastet,L., St-Pierre,P., Massé,E. and Lafontaine,D.A. (2011) Comparative study between transcriptionally- and translationally-acting adenine riboswitches reveals key differences in riboswitch regulatory mechanisms. *PLoS Genet.*, **7**, e1001278.
12. Blouin,S., Mulhbacher,J., Penedo,J.C. and Lafontaine,D.A. (2009) Riboswitches: ancient and promising genetic regulators. *Chembiochem.*, **10**, 400–416.
13. Schwalbe,H., Buck,J., Furtig,B., Noeske,J. and Wohnert,J. (2007) Structures of RNA switches: insight into molecular recognition and tertiary structure. *Angew. Chem. Int. Ed. Engl.*, **46**, 1212–1219.
14. Bunka,D.H.J. and Stockley,P.G. (2006) Aptamers come of age – at last. *Nat. Rev. Micro.*, **4**, 588–596.
15. Andrea,H., Soulière,M.F. and Micura,R. (2011) The dynamic nature of RNA as key to understanding riboswitch mechanisms. *Acc. Chem. Res.*, **44**, 1339–1348.
16. Lemay,J.F. and Lafontaine,D.A. (2007) Core requirements of the adenine riboswitch aptamer for ligand binding. *RNA*, **13**, 339–350.
17. Lemay,J.F., Penedo,J.C., Mulhbacher,J. and Lafontaine,D.A. (2009) Molecular basis of RNA-mediated gene regulation on the adenine riboswitch by single-molecule approaches. *Methods Mol. Biol.*, **540**, 65–76.

18. Noeske,J., Schwalbe,H. and Wöhnert,J. (2007) Metal-ion binding and metal-ion induced folding of the adenine-sensing riboswitch aptamer domain. *Nucleic Acids Res.*, **35**, 5262–5273.
19. Leipply,L. and Draper,D.A. (2011) Effects of Mg2+ on the free energy landscape for folding of a purine riboswitch RNA. *Biochemistry*, **50**, 2790–2799.
20. Serganov,A., Yuan,Y.R., Pikovskaya,O., Polonskaia,A., Malinina,L., Phan,A.T., Hobartner,C., Micura,R., Breaker,R.R. and Patel,D.J. (2004) Structural basis for discriminative regulation of gene expression by adenine- and guanine-sensing mRNAs. *Chem. Biol.*, **11**, 1729–1741.
21. Sharma,M., Bulusu,G. and Mitra,A.M.D. (2009) MD simulations of ligand-bound and ligand-free aptamer: molecular level insights into the binding and switching mechanism of the add A-riboswitch. *RNA*, **15**, 1673–1692.
22. Lemay,J.F., Penedo,J.C., Tremblay,R., Lilley,D.M.J. and Lafontaine,D.A. (2006) Folding of the adenine riboswitch. *Chem. Biol.*, **13**, 857–868.
23. Neupane,K., Yu,H., Foster,D.A.N., Wang,F. and Woodside,M.T. (2011) Single-molecule force spectroscopy of the add adenine riboswitch relates folding to regulatory mechanism. *Nucleic Acids Res.*, **39**, 7677–7687.
24. Greenleaf,W.J., Frieda,K.L., Foster,D.A.N., Woodside,M.T. and Block,S.M. (2008) Direct observation of hierarchical folding in single riboswitch aptamers. *Science*, **319**, 630–633.
25. Lin,J.C. and Thirumalai,D. (2008) Relative stability of helices determines the folding landscape of adenine riboswitch aptamers. *J. Am. Chem. Soc.*, **130**, 14080–14081.
26. Wakeman,C.A., Winkler,W.C. and Dann,C.E. 3rd (2007) Structural features of metabolite-sensing riboswitches. *Trends BioChem. Sci.*, **32**, 415–424.
27. Kim,J.N. and Breaker,R.R. (2008) Purine sensing by riboswitches. *Biol Cell*, **100**, 1–11.
28. Mulhbacher,J. and Lafontaine,D.A. (2007) Ligand recognition determinants of guanine riboswitches. *Nucleic Acids Res.*, **35**, 5568–5580.
29. Noeske,J., Richter,C., Grundl,M.A., Nasiri,H.R., Schwalbe,H. and Wöhnert,J. (2005) An intermolecular base triple as the basis of ligand specificity and affinity in the guanine- and adenine-sensing riboswitch RNAs. *Proc. Natl Acad. Sci. USA*, **102**, 132–1377.
30. Delfosse,V., Bouchard,P., Bonneau,E., Dagenais,P., Lemay,J.F., Lafontaine,D.A. and Legault,P. (2010) Riboswitch structure: an internal residue mimicking the purine ligand. *Nucleic Acids Res.*, **38**, 2057–2068.
31. Gilbert,S.D., Reyes,F.E., Edwards,A.L. and Batey,R.T. (2009) Adaptive ligand binding by the purine riboswitch in the recognition of purine and guanine analogs. *Structure*, **17**, 857–868.
32. De la Peña,M., Dufour,D. and Gallego,J. (2009) Three-way junctions with remote tertiary contacts: a recurrent and highly versatile fold. *RNA*, **15**, 1949–1964.
33. Batey,R.T., Gilbert,S.D. and Montage,R.K. (2004) Structure of a natural guanine-responsive riboswitch complexed with the metabolite hyponxanthine. *Nature*, **432**, 411–415.
34. Pikovskaya,O., Polonskaia,A., Patel,D.J. and Serganov,A. (2011) Structural principles of nucleoside selectivity in a 2'-deoxyguanosine riboswitch. *Nat. Chem. Biol.*, **7**, 748–755.
35. Stoddard,C.D., Gilbert,S.D. and Batey,R.T. (2008) Ligand-dependent folding of the three-way junction in the purine riboswitch. *RNA*, **14**, 675–684.
36. Jain,N., Zhao,L., Liu,J.D. and Xia,T. (2010) Heterogeneity and dynamics of the ligand recognition mode in purine-sensing riboswitches. *Biochemistry*, **49**, 3703–3714.
37. Prychyna,O., Dahabieh,M.S., Chao,J. and O'Neill,M.A. (2009) Sequence-dependent folding and unfolding of ligand-bound purine riboswitches. *Biopolymers*, **91**, 953–965.
38. Buck,J., Noeske,J., Wöhnert,J. and Schwalbe,H. (2010) Dissecting the influence of Mg^{2+} on 3D architecture and ligand-binding of the guanine-sensing riboswitch aptamer domain. *Nucleic Acids Res.*, **38**, 4143–4153.
39. Buck,J., Furtig,B., Noeske,J., Wöhnert,J. and Schwalbe,H. (2007) Time-resolved NMR methods resolving ligand-induced RNA folding at atomic resolution. *Proc. Natl Acad. Sci. USA*, **104**, 15699–15704.
40. Tremblay,R., Lemay,J.F., Blouin,S., Mulhbacher,J., Bonneau,E., Legault,P., Dupont,P., Penedo,J.C. and Lafontaine,D.A. (2011) Constitutive regulatory activity on an evolutionary excluded riboswitch variant. *J. Biol. Chem.*, **286**, 27406–27415.
41. Guo,Z., Karunatilaka,K.S. and Rueda,D. (2009) Single-Molecule Folding of Protein Free U2/U6 snRNAs. *Nat. Struct. Mol. Biol.*, **16**, 1154–1159.
42. Kuzmenkina,E.V., Heyes,C.D. and Nienhaus,G.U. (2005) Single-molecule Förster resonance energy transfer study of protein dynamics under denaturing conditions. *Proc. Natl Acad. Sci. USA*, **102**, 15741–15746.
43. Shelton,V.M., Sosnick,T.R. and Pan,T. (1999) Applicability of urea in the thermodynamic analysis of secondary and tertiary RNA folding. *Biochemistry*, **38**, 16831–16839.
44. Sosnick,T.R. and Pan,T. (2003) RNA folding: models and perspectives. *Curr. Opin. Struct. Biol.*, **13**, 309–316.
45. Bartley,L.E., Zhuang,X., Das,R., Chu,S. and Herschlag,D. (2003) Exploration of transition state for tertiary structure formation between an RNA helix and large structured RNA. *J. Mol. Biol.*, **328**, 1011–1026.
46. Treiber,D.K., Rook,M.S., Zarrinkar,P.P. and Williamson,J.R. (1998) Kinetic intermediates trapped by native interactions in RNA folding. *Science*, **279**, 1943–1946.
47. Pan,T. and Sosnick,T.R. (1997) Intermediate and kinetic traps in the folding of a large ribozyme revealed by circular dichroism and UV absorbance spectroscopies and catalytic activity. *Nat. Struct. Biol.*, **4**, 931–938.
48. Bokinsky,G., Rueda,D., Misra,V.K., Rhodes,M.M., Gordus,A., Babcock,H.P., Walter,N.G. and Zhuang,X. (2003) Single-molecule transition-state analysis of RNA folding. *Proc. Natl Acad. Sci. USA*, **100**, 9302–9307.
49. Hurton,T.E. and DeRose,V.J. (2000) Cobalt hexammine inhibition of the *Hammerhead Ribozyme*. *Biochemistry*, **39**, 11408–11416.
50. Lambert,D. and Draper,D.E. (2012) Denaturation of RNA secondary and tertiary structure by urea: simple unfolded state models and free energy parameters account for measured m-values. *Biochemistry*, **51**, 9104–9026.
51. Mikulecky,P.J. and Feig,A.L. (2002) Cold denaturation of the hammerhead ribozyme. *J. Am. Chem. Soc.*, **13**, 890–891.
52. Kurzban,G.P., Bayer,E.A., Wilchek,M. and Horowitz,P.M. (1991) The quaternary structure of streptavidin in urea. *J. Biol. Chem.*, **266**, 14471–14477.
53. Eskandari,S., Prychya,O., Leung,J., Avdic,D. and And O'Neill,M. (2007) Ligand-directed dynamics of adenine riboswitch conformers. *J. Am. Chem. Soc.*, **129**, 11308–11309.
54. Gilbert,S.D., Stoddard,C.D., Wise,S.J. and Batey,R.T. (2006) Thermodynamic and kinetic characterization of ligand binding to the purine riboswitch aptamer domain. *J. Mol. Biol.*, **359**, 754–768.
55. Heppell,B., Blouin,S., Dussault,A.M., Mulhbacher,J., Ennifar,E., Penedo,J.C. and Lafontaine,D.A. (2011) Molecular insights into the ligand-controlled organization of the SAM-I riboswitch. *Nat. Chem. Biol.*, **7**, 384–392.
56. Rieder,U., Haller,A., Aigner,M., Blanchard,S.C. and Micura,R. (2011) Conformational capture of the SAM-II riboswitch. *Nat. Chem. Biol.*, **7**, 393–400.
57. Duchardt-Ferner,E., Weigand,J.E., Ohlenschlager,O., Schmidtke,S.R., Suess,B. and Wohnert,J. (2010) Highly modular structure and ligand binding by conformational capture in a minimalistic riboswitch. *Angew. Chem. Int. Ed.*, **49**, 6216–6219.
58. Brooks,K.M. and Hampel,K.J. (2009) A rate-limiting conformational step in the catalytic pathway of the *glms* ribozyme. *Biochemistry*, **48**, 5669–5678.
59. Priyakumar,U.D., Hyeon,C., Thirumalai,D. and Mackerell,A.D. Jr (2009) Urea destabilizes RNA by forming stacking interactions and multiple hydrogen bonds with nucleic acids. *J. Am. Chem. Soc.*, **131**, 17759–17761.
60. Gilbert,S.D. and Batey,R.T. (2006) Riboswitches: fold and function. *Chem. Biol.*, **13**, 805–807.
61. Huang,L., Serganov,A. and Patel,D.J. (2009) Structural insights into ligand recognition by a sensing domain of the cooperative glycine riboswitch. *Mol. Cell*, **40**, 774–786.
62. Thore,S., Leibundgut,M. and Ban,N. (2006) Structure of the thiamine pyrophosphate riboswitch with its regulatory ligand. *Science*, **312**, 1208–1211.